BIOCHEMISTRY
including biophysical chemistry & molecular biology

ARTICLE

pubs.acs.org/biochemistry

Regulation of Insulin-Regulated Membrane Aminopeptidase Activity by Its C-Terminal Domain

David B. Ascher,[†] Brett A. Cromer,[†] Craig J. Morton,[†] Irene Volitakis,[‡,§] Robert A. Cherny,[‡,§] Anthony L. Albiston,[∥] Siew Yeen Chai,[∥] and Michael W. Parker*[,†,⊥]

[†]Centre for Structural Neurobiology and Biota Structural Biology Laboratory, St. Vincent's Institute, 9 Princes Street, Fitzroy, Victoria 3065, Australia

[‡]Department of Pathology, The University of Melbourne, Parkville, Victoria 3010, Australia

[§]The Mental Health Research Institute of Victoria, Parkville, Victoria 3052, Australia

[∥]Howard Florey Institute of Experimental Medicine and Physiology, The University of Melbourne, Parkville, Victoria 3010, Australia

[⊥]Department of Biochemistry and Molecular Biology, Bio21 Molecular Science and Biotechnology Institute, The University of Melbourne, 30 Flemington Road, Parkville, Victoria 3010, Australia

Supporting Information

ABSTRACT: The development of inhibitors of insulin-regulated aminopeptidase (IRAP), a membrane-bound zinc metallopeptidase, is a promising approach for the discovery of drugs for the treatment of memory loss such as that associated with Alzheimer's disease. There is, however, no consensus in the literature about the mechanism by which inhibition occurs. Sequence alignments, secondary structure predictions, and homology models based on the structures of recently determined related metallopeptidases suggest that the extracellular region consists of four domains. Partial proteolysis and mass spectrometry reported here confirm some of the domain boundaries. We have produced purified recombinant fragments of human IRAP on the basis of these data and examined their kinetic and biochemical properties. Full-length extracellular constructs assemble as dimers with different nonoverlapping fragments dimerizing as well, suggesting an extended dimer interface. Only recombinant fragments containing domains 1 and 2 possess aminopeptidase activity and bind the radiolabeled hexapeptide inhibitor, angiotensin IV (Ang IV). However, fragments lacking domains 3 and 4 possess reduced activity, although they still bind a range of inhibitors with the same affinity as longer fragments. In the presence of Ang IV, IRAP is resistant to proteolysis, suggesting significant conformational changes occur upon binding of the inhibitor. We show that IRAP has a second Zn^{2+} binding site, not associated with the catalytic region, which is lost upon binding Ang IV. Modulation of activity caused by domains 3 and 4 is consistent with a conformational change regulating access to the active site of IRAP.

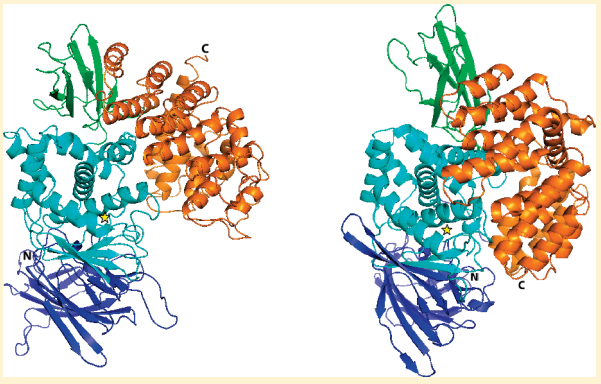

Insulin-regulated aminopeptidase (IRAP), also known as the AT_4 receptor[1] or oxytocinase,[2] plays a number of important but diverse roles in the body. While it was first implicated in the regulation of parturition through the proteolysis of the uterogenic peptide oxytocin, IRAP has subsequently been implicated in diabetes, the immune system, and memory.[3−5] A range of ligands originally described as AT_4 agonists, including angiotensin IV (Ang IV) and LVV-hemophin-7 (LVV-H7), have subsequently been shown to inhibit the aminopeptidase activity of IRAP.[1,6,7] When administered intracranially, these inhibitors have been shown to greatly enhance memory and cognitive function in normal rodents[8,9] and reverse memory deficits in animal models of amnesia.[10−13] These effects are likely to be mediated through the inhibition of degradation of endogenous neural promnestic peptides because several IRAP substrates such as vasopressin, CCK-8, oxytocin, and somatostatin have been shown to facilitate learning and memory in animal models (see ref 14 for a review). A number of alternative mechanisms for explaining the cognitive improvement have also been proposed.[15] The importance of IRAP in memory has been strikingly demonstrated recently with the report of novel and highly specific small molecule inhibitors.[16] When tested in vivo, the compounds were able to improve cognitive function in animals. This work provided compelling evidence of the role of IRAP in

Received: November 28, 2010
Revised: February 20, 2011
Published: February 24, 2011

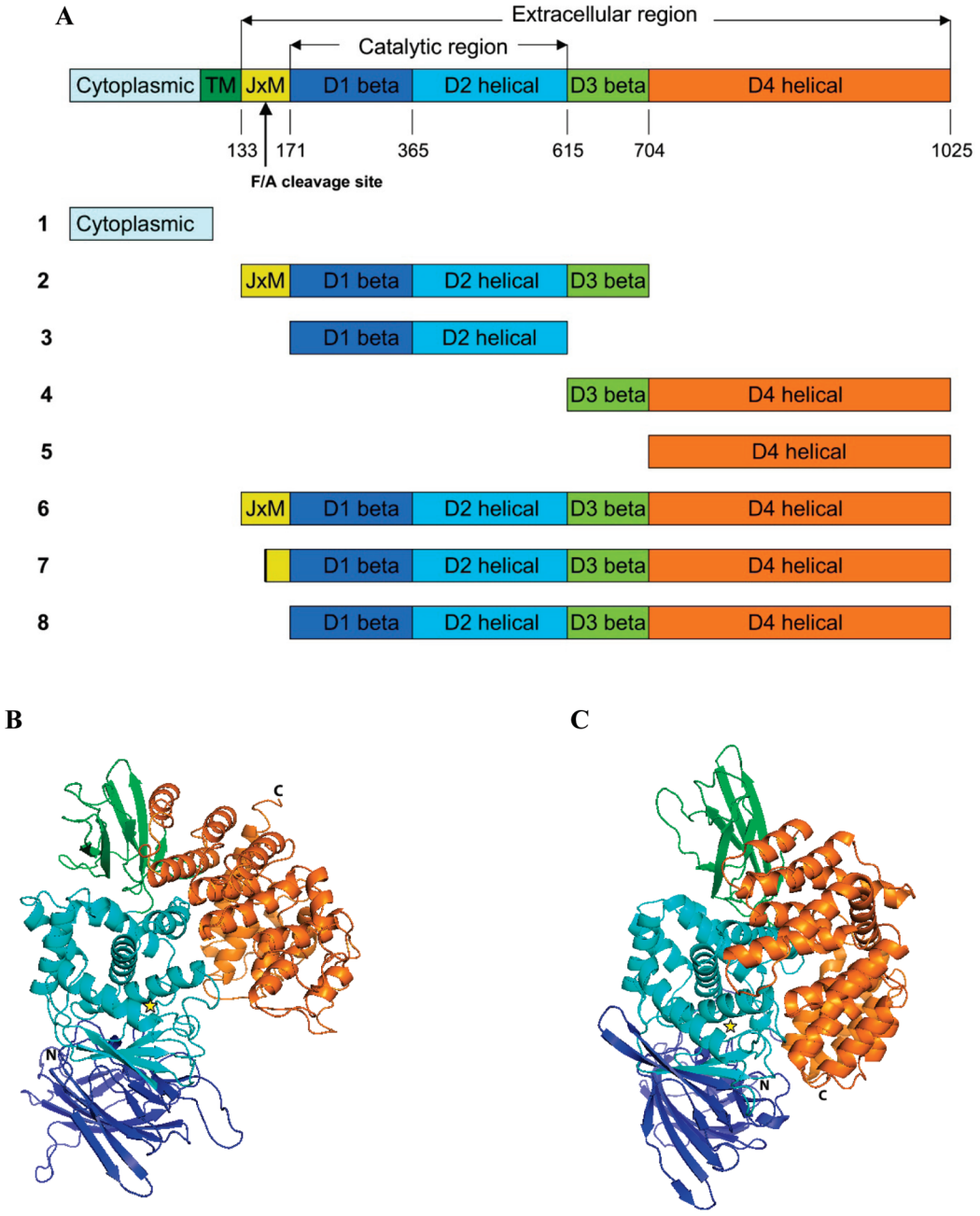

Figure 1. IRAP domain structure. (A) Schematic diagram of the proposed domain boundaries and the different constructs expressed in insect cells. (B and C) Ribbon representations of the homology models of the extracellular region of IRAP based upon the crystal structures of Tricorn Interacting Factor F3 and APN, respectively. Panel B shows a putative model of the open state and panel C the closed state of IRAP. The models are colored according to putative domains using the same coloring scheme as shown in panel A. The N- and C-termini are labeled, and the approximate location of the active site is denoted with a star.

improving cognitive function through inhibition of its enzymatic activity.

IRAP belongs to the M1 family of zinc metallopeptidases.[2] This class of enzymes is characterized by two common structural features: a Zn^{2+} binding motif [$HEXXH(X)_{18}$-E] and an exopeptidase motif (GXMEN). IRAP is a type II membrane-spanning protein with an extracellular catalytic site and a putative cleavage site (F^{154}/A^{155}) for release of the extracellular region of IRAP,[17,18] with ADAM12 reported to be responsible for this cleavage.[19] Several groups have looked at IRAP inhibition using a range of techniques and have proposed three different mechanisms of inhibition. First, on the basis of the kinetics of inhibition, we have previously proposed that inhibitors such as Ang IV inhibit IRAP activity directly through competitive inhibition.[6,20] Second, it has also been reported that Ang IV interacts with a juxtamembrane site of IRAP and that Ang IV may use an allosteric mechanism to modulate IRAP activity.[21] Finally, it has been reported that Ang IV binds with high affinity only to the Zn^{2+}-depleted apoenzyme and may inhibit IRAP activity by stabilizing an inactive apoenzyme form.[22−24] While these conclusions are not necessarily mutually

exclusive, it highlights the fact that further work is required to understand the mechanism behind inhibition and regulation of IRAP activity.

Considering the wide-ranging effects mediated by IRAP and its inhibitors, an understanding of IRAPs biochemical mechanism of action and inhibition will help guide the design of more potent physiologically stable inhibitors. Here we define the essential regions of human IRAP required for aminopeptidase activity, inhibition, and regulation leading to a model that rationalizes these and previously published observations.

MATERIALS AND METHODS

Bioinformatics Analyses. Sequence alignments of analogous and homologous sequences of human IRAP were identified by psi-BLAST[25] and were performed using ClustalW[26] and Fugue[27] and viewed using ALSCRIPT[28] and ESPRIPT.[29] Secondary structure predictions were performed using a variety of programs, including APSSP2,[30] JUFO,[31] PHDSec,[32] PRED-TMR2,[33] PsiPred,[34] and SSpro.[35] Potential transmembrane regions were predicted using HMMTOP,[36] PredictProtein, SOSUI,[37] TMAP,[38] TMHMM,[39] and TMpred.[40] A consensus result was recorded in each analysis in which there was more than 70% agreement by all methods tested.

Expression and Purification. Seven different constructs covering the entire extracelluar region of human IRAP were expressed in insect cells, secreted into the media, and purified as described in detail elsewhere (D. B. Ascher et al., manuscript in preparation). Briefly, the boundaries chosen were based upon bioinformatics analysis (Figure 1 and Figure S1 of the Supporting Information) and the constructs expressed with His or MBP-His tags followed by a TEV protease site for removal of the tags. Site-directed mutagenesis was performed using the Stratagene QuikChange II XL Site-Directed Mutagenesis Kit according to the manufacturer's instructions. All constructs were sequenced by the Sequencing Facility of the Department of Pathology, The University of Melbourne. Following baculoviral expression, the medium was concentrated and buffer-exchanged into 500 mM NaCl, 100 mM maltose, 25 mM Tris-HCl, and 20 mM imidazole (pH 6.8−7.2), and batch-purified using Qiagen Ni-NTA Superflow resin. The tags were removed from the constructs by incubation with recombinant His-tagged TEV. The tags and tagged TEV were then removed by incubation with Ni-NTA resin. The purified proteins were dialyzed into 25 mM Tris-HCl (pH 6.8−7.2) and 150 mM NaCl and concentrated. The individual domain constructs were also expressed with a GST tag for use in pull-down assays. The majority of these latter constructs were incorrectly processed; the fractions containing the correctly secreted protein were purified by incubation with GSH resin from Novagen. A range of mutations were introduced into constructs 6 and 7 (Figure 1) using the QuickChange II XL Site-Directed Mutagenesis Kit (Stratagene).

Size Exclusion Chromatography. The approximate molecular mass and oligmerization state of the purified proteins were estimated by size exclusion chromatography using a GE Akta Express fitted with a Sephedex 200 10/300HL column and using a mobile phase consisting of 25 mM Tris-HCl (pH 7.1) and 150 mM NaCl. Calibration was performed using the High MWt Calibration Kit from GE Healthcare ($r^2 > 0.99$).

Dynamic Light Scattering. The oligomerization states of the purified constructs were analyzed by dynamic light scattering using a Malvern Instruments Zetasizer Nano ZS instrument. The GE Healthcare High MWt Calibration Kit was used for standards.

Pull-Downs. For pull-down assays, purified His-tagged D1+D2 and GST-tagged D4 were bound to Ni-NTA and glutathione resin, respectively. Unbound protein was washed off in 150 mM NaCl, 20 mM imidazole, and 25 mM Tris-HCl (pH 7.2). The resins were then incubated at 4 °C for 1−2 h with untagged D1+D2 or D4. As controls, untagged D1+D2 and D4 were also incubated with Ni-NTA and glutathione resin alone to ensure they did not interact directly with the resins (data not shown). Unbound protein was once again washed off in 150 mM NaCl, 20 mM imidazole, and 25 mM Tris (pH 7.2), and the beads were resuspended in 1× SDS protein sample buffer and analyzed on a 4 to 12% (w/v) acrylamide gel.

Enzyme Activity and Inhibition Assay. The catalytic activity of the recombinant products was determined by the hydrolysis of a synthetic fluorogenic substrate, L-leucine-4-methylcoumaryl-7-amide (MCA), in a microtiter plate assay (as described in ref 41). The potency of each inhibitor was determined over a range of concentrations and at multiple substrate concentrations, with each concentration assayed in triplicate. The k_{cat} and K_m values were calculated using Michaelis−Menten kinetics by nonlinear regression using GraphPad Prism (GraphPad Software Inc., San Diego, CA). The inhibition data were fitted with GraphPad Prism using nonlinear regression to equations for competitive $[Y = (V_{max}X)/(K_{mapp} + X)]$, noncompetitive $[Y = (V_{maxinh}X)/(K_m + X)]$, uncompetitive $[Y = (V_{maxapp}X)/(K_{mapp} + X)]$, and mixed $[Y = (V_{max}X)/(K_{mapp} + X\{1 + [I/(AK_i)]\})]$ inhibition models. The inhibition constants were also determined from the linear secondary plots (data not shown). The temperature stability of each construct was determined by incubating the purified protein at the temperature of interest (4−55 °C) overnight. The activity was then measured as described above. The pH sensitivity of each construct was determined by dialyzing the purified protein into the pH of interest (pH 4−10) using Slide-A-Lyzer Mini Dialysis Units (Pierce) and the activity measured as described above. Each replicate (n) is a separate protein preparation measured in triplicate. All analyses were repeated a minimum of three times (n = 3). Significant differences were examined by one-way Anova with a Tukey posthoc test.

Radioligand Binding Assay. The published method for determining competitive and saturation kinetics of IRAP[42] was modified to take into account the fact that this study has used purified protein rather than partially purified membrane preparations. Purified protein in 25 mM Tris-HCl (pH 7.2) and 150 mM NaCl was incubated with [^{125}I]Nle^1-Ang IV (specific activity of 2175 Ci/mmol) in the presence of 100 μM 1,10-phenanthroline and 5 mM EDTA. For saturation binding studies, up to 10 pmol of purified protein was incubated with increasing concentrations (up to 20 nM) of [^{125}I]Nle^1-Ang IV for 2 h at 37 °C, and nonspecific binding was assessed in the presence of 10 μM unlabeled Ang IV. For competition binding studies, 5 pmol of purified protein was incubated with 0.5 μCi/mL [^{125}I]Nle^1-Ang IV and increasing concentrations of unlabeled Nle^1-Ang IV and Ang IV for 2 h at 37 °C. For both competition and saturation binding studies, bound radioligand and free radioligand were separated using Illusra MicroSpin G-25 columns (GE Healthcare), pre-equilibrated in binding buffer. The radioligand binding data were analyzed via an iterative, model fitting program on GraphPad Prism (GraphPad Software Inc.), with K_d and B_{max} derived using the equation $Y = (B_{max}X)/(K_d + X)$ and K_i derived using the equation $K_i = IC_{50}/(1 + [S]/K_d)$. Each replicate ($n$) is a separate protein preparation measured in triplicate. All analyses were repeated a minimum of three times

Table 1. Biochemical Properties of Fragments

		ICP-MS (n = 3)		radioligand saturation binding (n = 3 at three different protein concentrations)		radioligand competitive binding (n = 3)	
construct (domains)	oligomerization (n = 2)	Zn content (mol of zinc/mol of protein)	Zn content (mol of zinc/mol of monomer) in the presence of Ang IV	K_d of [^{125}I]Nle^1-Ang IV (nM)	B_{max} of [^{125}I]Nle^1-Ang IV (pmol of [^{125}I]Nle^1-Ang IV/pmol of protein)	K_i of Nle^1-Ang IV (nM)	K_i of Ang IV (nM)
1 (Cyto)	monomer	0.03 ± 0.01[a]	0.01 ± 0.02[a]		no detectable binding		
2 (JxM, D1−D3)	dimer	0.89 ± 0.11[a]	0.91 ± 0.08	0.63 ± 0.07	0.87 ± 0.16	1.4 ± 0.3	16 ± 2.3
3 (D1, D2)	dimer	0.92 ± 0.09[a]	0.89 ± 0.17	0.57 ± 0.12	0.95 ± 0.09	1.2 ± 0.4	16 ± 1.8
4 (D3, D4)	dimer	1.04 ± 0.18[a]	1.02 ± 0.17		no detectable binding		
5 (D4)	dimer	0.98 ± 0.15[a]	1.06 ± 0.11		no detectable binding		
6 (JxM, D1−D4)	dimer	1.98 ± 0.04	1.12 ± 0.18[b]	0.72 ± 0.09	1.08 ± 0.05	1.3 ± 0.3	17 ± 1.2
7 (F/A, D1−D4)	dimer	2.03 ± 0.07	0.98 ± 0.09[b]	0.78 ± 0.14	0.94 ± 0.08	1.5 ± 0.2	16 ± 0.8
8 (D1−D4)	dimer	2.02 ± 0.06	1.09 ± 0.15[b]	0.76 ± 0.08	1.09 ± 0.08	1.4 ± 0.2	17 ± 1.4

[a] $p < 0.001$ compared to that for construct 6. [b] $p < 0.001$ compared to that in the absence of Ang IV.

(n = 3), and significant differences were examined by one-way Anova with a Tukey posthoc test.

Proteolytic Fragmentation. Protease digestions by proteinase K, chymotrypsin, and trypsin were conducted in 50 mM Tris-HCl buffer (pH 7.2) containing 150 mM NaCl in the presence and absence of 500 nM Ang IV at 37 °C for 2 h. The reactions were stopped by either the addition of sample loading buffer and boiling for 5 min prior to analysis by sodium dodecyl sulfate−polyacrylamide gel electrophoresis (SDS−PAGE) or the addition of PMSF to a final concentration of 0.5 mM for proteinase K and chymotrypsin digests or soybean trypsin inhibitor for trypsin digests.

ESI-MS and TOF-MS. Proteolyzed fragments, obtained by partial trypsin proteolysis, were deglycosylated using PNGaseF to obtain adequate sequence coverage. The Sigma-Aldrich Trypsin Profile IGD Kit was then used to generate tryptic peptides for MS analysis. Samples were run on an Agilent 6510 Q-TOF LC/MS instrument using a C18 column to help separate peptides and an Agilent 6340 Ion Trap LC/MS instrument using an Agilent HPLC chip (40 nL enrichment column, 150 mm × 75 μm analytical column with 5 μm C18 Zorbax resin). Experimental peptide masses and MS/MS fragmentation were then compared to the predicted peptide masses by the Expasy webtool PeptideMass (http://au.expasy.org/tools/peptide-mass.html[43]).

Inductively Coupled Plasma Mass Spectrometry (ICP-MS) for the Analysis of Metal Content. Samples (200 μg) were incubated, with and without Ang IV (0, 100, 250, 500, and 1000 nM), at room temperature for 1 h (for comparisons, only data for 0 and 250 nM are presented). The protein was then isolated by being run through an Illusra MicroSpin G-25 column (GE Healthcare), pre-equilibrated in sample buffer, and then concentrated. Samples (at 1 mg/mL) were diluted in a 1% (v/v) HNO_3 solution for analysis by ICP-MS. ICP-MS was performed using an Ultramass 700 instrument (Varian, Victoria, Australia). Levels of Fe and Cu ions measured were not significant in any of the samples tested. Each replicate is of a different protein preparation, and significant differences were analyzed by one-way Anova with a Tukey posthoc test.

Molecular Modeling of IRAP. The crystal structures of two closely related M1 aminopeptidases have been determined: *Thermoplasma acidophilum* Tricorn Interacting Factor F3 (Protein Data Bank entry 1Z5H[44]) and *Escherichia coli* aminopeptidase N (APN) (Protein Data Bank entry 2DQ6[45]). While the overall degree of similarity between the sequences is low (21−25% identical in pairwise sequence and 38−46% similar in sequence to IRAP), the region immediately surrounding the active site residues, including the HEXXH and GXMEN motifs, is relatively well conserved (23−35% identical in pairwise sequence and 42−55% similar in sequence to IRAP), and some significant sequence similarity can be seen in the C-terminal regions (e.g., ∼33% similarity between Tricorn vs IRAP). A sequence alignment of several different members of the M1 aminopeptidase family along with predicted secondary structure was used to guide model building (Figure S1 of the Supporting Information). The models (open and closed states) were built using Swiss PDB Viewer[46] and minimized in Sybyl under the Tripos force field (Tripos, St. Louis, MO). Zn^{2+} was manually added to the active site motif after comparison with the Zn^{2+}-bound structures of aminopeptidase N and Tricorn Interacting Factor F3 indicated the conformation of residues in the Zn^{2+} binding motif was identical among the proteins. The quality of the models was analyzed with Verify3D,[47] which indicated that the models were of good quality (data not shown).

Statistical Analyses. All statistical analyses were performed using GraphPad Prism (GraphPad Software Inc.). Each replicate is for a separate protein preparation measured three times.

RESULTS

Design of Constructs. We predicted that IRAP is composed of six distinct regions on the basis of sequence alignments and

domain and secondary structure prediction programs (Figure 1A and Figure S1 of the Supporting Information): a cytoplasmic region (residues 1−110), a typical α-helical transmembrane region (TM, residues 111−133) followed by a small juxtamembrane region (JxM) of undefined structure, a β-sheet region (D1, residues 171−365), and two α-helical regions (D2, residues 365−615, and D4, residues 704−1025) separated by another β-sheet region (D3, residues 615−704). D1+D2 consists of the catalytic domains that contain the HEXXH(X)$_{18}$E Zn^{2+} binding motif and the GAMEN exopeptidase motif. Eight distinct constructs were designed on the basis of this breakdown (Figure 1). These were successfully expressed in insect cells, and all extracellular constructs were efficiently secreted into the media.

The crystal structures of three related zinc aminopeptidases have been determined: LTA4H,[48] Tricorn Interacting Factor F3,[44] and APN.[45,49] On the basis of these structures, we have generated several molecular models of the extracellular region of IRAP. Initially, we had built a model of the catalytic region on the crystal structure of LTA4H.[16,50] At the time, the C-terminal region could not be modeled because of the very low level of sequence similarity: sequence alignments suggested that LTA4H lacked D3 and a significant proportion of D4. Following the publication of the crystal structures of Tricorn Interacting Factor F3 and *E. coli* APN, we were able to model the entire extracellular region of IRAP in open and closed states (Figure 1B,C). While the secondary structural alignment of these two extracellular region models was consistent, the relative positioning of the individual domains was quite distinct. The models of the extracellular region of IRAP are limited by the fact that the level of sequence similarity and hence reliability of the model decrease toward the C-terminal end of the molecule. Regardless, the homology models are consistent with the bioinformatics predictions of the different structural regions (D1−D4). All the models suggest that D1 and D2 form a tight interface while D3 and D4 form more distinct independent units.

The IRAP Extracellular Region Dimerizes and Is Comprised of Separable Stable Domains. The purified constructs were analyzed by size exclusion chromatography (SEC) and dynamic light scattering, under native nonreducing conditions. The full-length constructs eluted in a nearly homogeneous peak with a molecular weight consistent with a dimerized state (Table 1). Recombinant IRAP was completely dimerized even in the presence of 5 mM DTT and also in constructs lacking the key cysteine residues (C134 and C141) responsible for dimerization in the related M1 aminopeptidases APA and TRH-DE.[51−53] This indicated that intermolecule disulfide formation is not required for dimerization of IRAP. To examine whether an intermolecular disulfide is present, the purified constructs were subjected to SDS−PAGE in the presence and absence of DTT. For all purified extracellular constructs, a weak band with a molecular weight consistent with a dimer of IRAP was always observed. A difference between the samples run in the presence and absence of DTT was observed only in the constructs containing the juxtamembrane region (which contains C134 and C141), where in the absence of DTT a higher percentage of dimerized product was observed (data not shown). To examine any effect that binding of inhibitors may have on IRAP's dimerization, with potential implications for intracellular signaling, SEC was conducted in the presence of Ang IV. However, no differences were observed. As Ang IV has been proposed to bind to only the apo form of IRAP,[22,23,54,55] the effects of the metal chelator 1,10-phenanthroline were also examined in the presence and absence of Ang IV. Once again, the extracellular regions were predominantly dimers in the presence of 1,10-phenanthroline, with or without Ang IV.

D1+D2 and D4 constructs formed homodimers independently of each other (Table 1), though a higher proportion of monomer was observed for the separate domains than for the full-length construct. Thus, D1+D2 and D4 appear to contain sufficient information on their own for homodimerization, suggesting an extended dimer interface between IRAP molecules.

When expressed for an extended period of time, the His-tagged full length extracellular constructs were degraded in insect cell media to a stable protein approximately half the size of the full-length construct. This fragment still contained its hexameric His tag, indicating that proteolysis was removing part of the C-terminal end of the protein. These observations were further explored by subjecting purified full-length constructs to a range of proteolytic enzymes, which repeatedly showed that partial proteolysis yielded two stable fragments, one with a His tag and the other without (Figure S2 of the Supporting Information). The boundaries of these stable fragments were examined by mass spectroscopy of in-gel tryptically digested peptides, which suggested that the fragments corresponded to residues 168−560 and 718−1016 (Table S1 of the Supporting Information). While tryptic peptides from the D3 region could be observed in the full-length construct, they were not observed in the partially proteolyzed fragments, suggesting that the His-tagged fragment corresponded to D1+D2 and the other fragment corresponded to D4. This proteolyzed protein, purified using the His tag at the N-terminus, was more stable to temperature and proteolysis than the catalytic domain construct containing D3 and was also shown to run as a dimer on SEC (Table 1).

Interaction between Catalytic and C-Terminal Domains. There was some evidence of heterodimer formation, as judged by SEC, when purified D1+D2 and D4 fragments were mixed together. A small amount of a higher-order complex was also evident by both SEC and Coomassie stain, consistent with formation of a heterotetramer consisting of two D1+D2 and two D4 fragments. Pull-down experiments were conducted to further analyze and characterize these complexes. Purified, untagged D1+D2 and D4 proteins were mixed with the equivalent His-tagged proteins over the IMAC resin and the isolated proteins analyzed via SDS−PAGE. The hexa-His-tagged D1+D2 constructs were able to pull down purified untagged D1+D2 and D4, while conversely, the GST-tagged D4 was able to pull down purified untagged D1+D2 and D4 (Figure S2 of the Supporting Information).

When partial proteolysis was performed in the presence of Ang IV, the intact extracellular region construct was resistant to proteolysis with less than 50% breakdown after 90 min compared to nearly complete proteolysis over the same time period in the absence of ligand. This is consistent with the hypothesis that upon binding of Ang IV the extracellular region of IRAP undergoes a conformational change that makes it less susceptible to proteolysis.

The Catalytic Domain Is Sufficient for Catalytic Activity and Ang IV Inhibition. We predicted that D1+D2 alone would contain all of the structural information necessary for activity, and thus, all constructs containing D1+D2 should be active. Our data confirmed this hypothesis but also revealed that the specific activity of D1+D2 was significantly lower than that of the entire extracellular region (Figure 2A and Table 2). While the K_m values of all the active constructs was approximately the same, the V_{max}

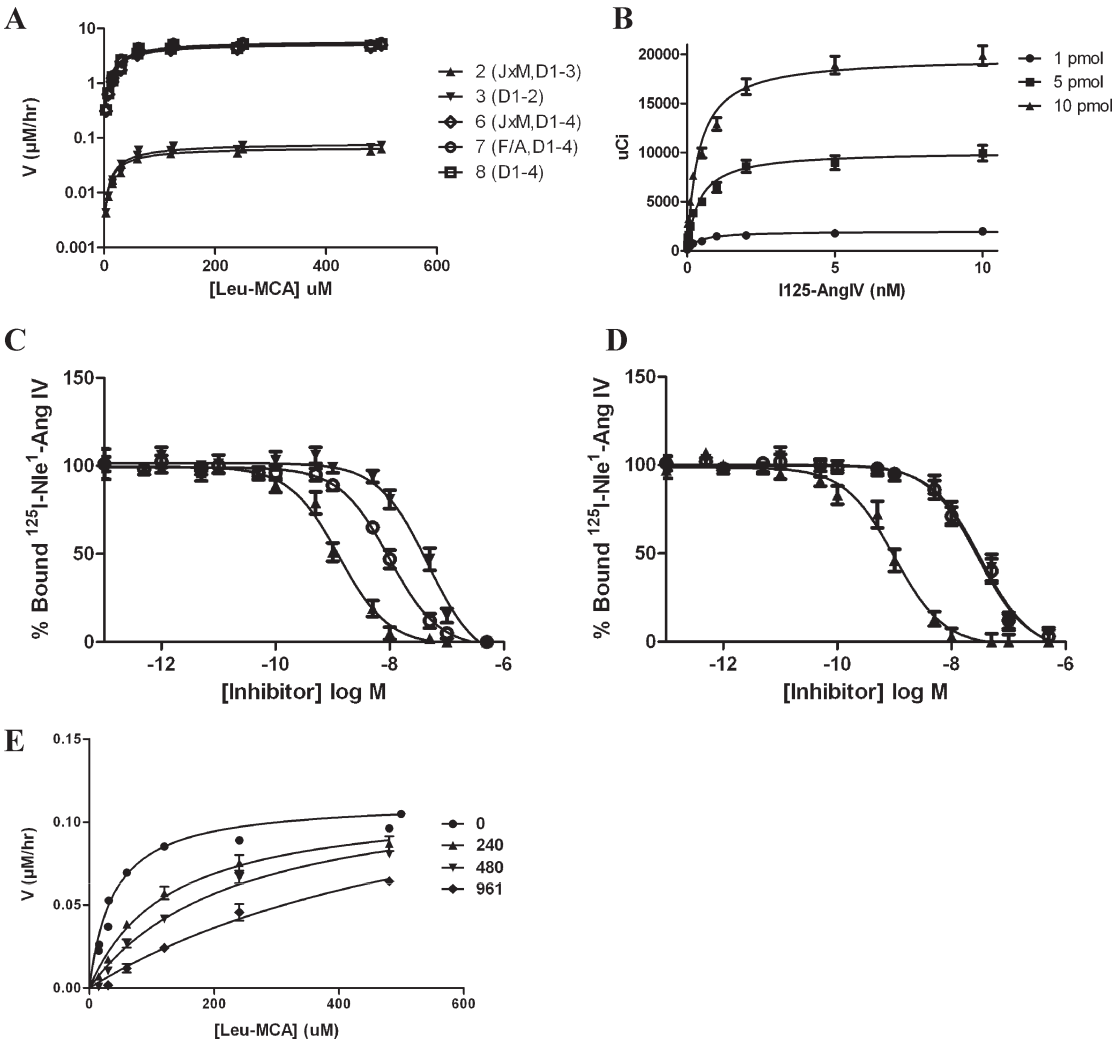

Figure 2. Kinetic and binding curves. (A) Aminopeptidase activity of the purified constructs measured by following Leu-MCA degradation. (B) Saturation binding of [^{125}I]Nle^1-Ang IV to construct 7 (F/A, D1−D4) at three different protein concentrations. Competitive binding of Ang IV in the presence and absence of 1 mM DTT (▼ and ○, respectively) and Nle^1-Ang IV (▲) to constructs 7 [F/A, D1−D4 (C)] and 3 [D1+D2 (D)]. (E) Inhibition of the aminopeptidase activity of construct 3 (D1+D2) by Ang IV. The concentration in nanomolar is shown for each symbol.

Table 2. Kinetic Constants of Fragments

construct (fragments)	K_m for MCA (μM) (n = 3)	K_{cat} for MCA (s^{-1})	K_m for MCA with 1 mM DTT (μM) (n = 3)	K_{cat} for MCA with 1 mM DTT (s^{-1})	K_i for Ang IV (nM) (n = 3)	K_i for LVV-H7 (nM) (n = 3)	K_i for amastatin (μM) (n = 3)	K_i for bestatin (μM) (n = 3)	K_i for HFI419 (μM) (n = 3)	K_i for HFI435 (μM) (n = 3)	K_i for HFI437 (μM) (n = 3)
2 (JxM, | D1−D3)	35.2 ± 3.0	0.29 ± 0.05[a]	33.0 ± 2.0[a]	0.22 ± 0.09[a]	113 ± 3.7	859 ± 32	1.2 ± 0.12	222 ± 8.2	0.42	0.34	0.02
3 (D1, D2)	36.7 ± 1.2	0.33 ± 0.03[a]	34.5 ± 1.8[a]	0.34 ± 0.06[a]	113 ± 3.3	857 ± 29	1.3 ± 0.11	225 ± 7.6	0.43	0.33	0.01
6 (JxM, D1−D4)	39.7 ± 0.82	14.1 ± 0.52	25.7 ± 0.73[c]	21.6 ± 1.6[c]	117 ± 2.3	847 ± 22	1.5 ± 0.09	233 ± 7.5	0.46	0.36	0.02
7 (F/A, D1−D4)	38.8 ± 2.3	15.2 ± 0.97	26.1 ± 0.82[c]	22.0 ± 2.2[c]	117 ± 2.8	849 ± 17	1.4 ± 0.08	231 ± 6.3	0.48	0.36	0.02
8 (D1−D4)	38.9 ± 2.0	14.7 ± 0.87	26.1 ± 0.75[c]	22.4 ± 2.0[c]	118 ± 3.2	851 ± 23	1.5 ± 0.08	232 ± 7.1	0.46	0.38	0.02
3 (D1, D2) mixed with 5 (D4)	35.8 ± 1.5	1.53 ± 0.06[a]	30.3 ± 1.44[b]	2.5 ± 0.47[a]	115 ± 2.8	852 ± 22	1.4 ± 0.11	228 ± 8.3			

[a] $p < 0.001$ compared to that for construct 6. [b] $p < 0.05$ compared to that in the absence of DTT. [c] $p < 0.001$ compared to that in the absence of DTT.

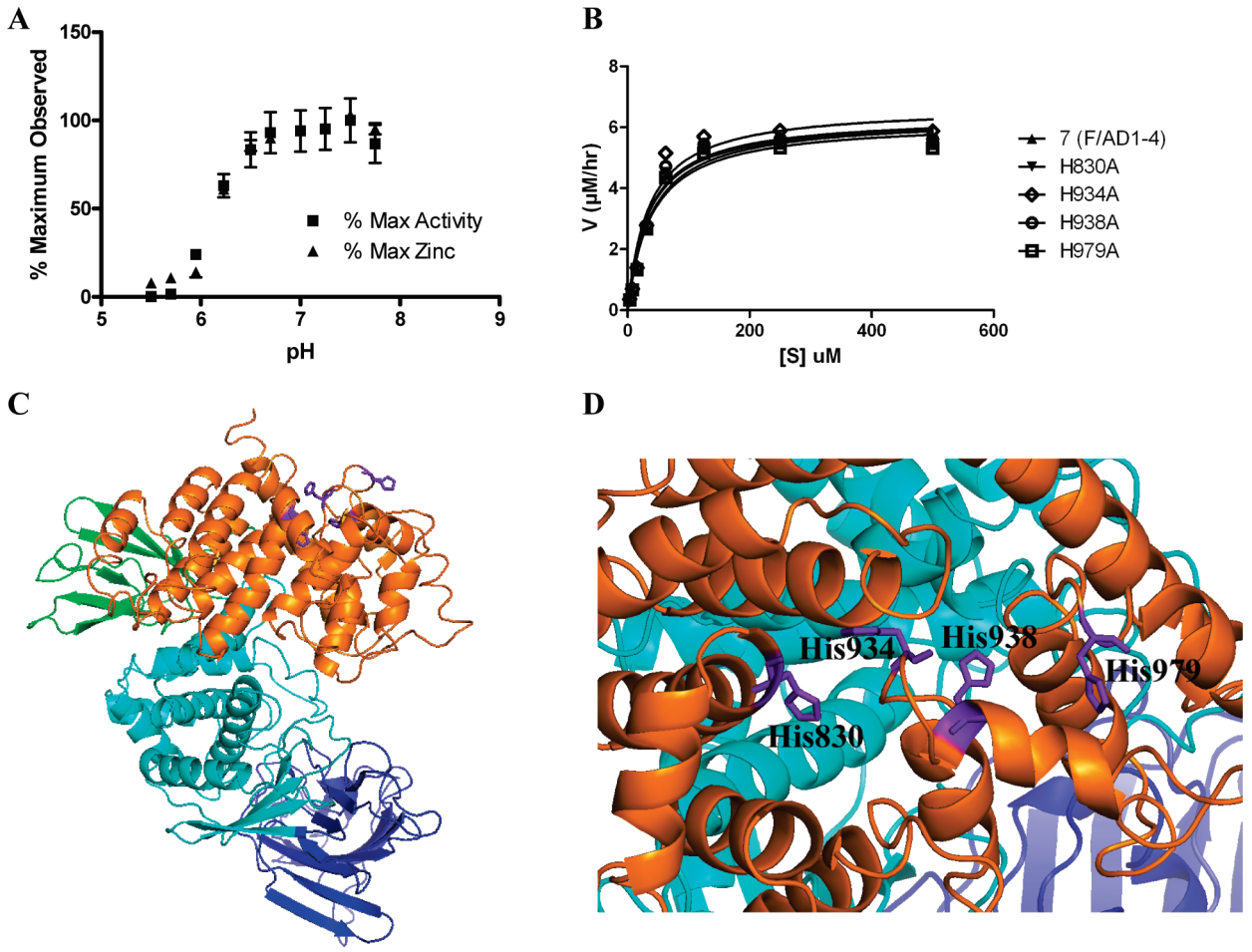

Figure 3. Second zinc binding site. (A) pH dependence of activity and zinc binding [shown here for construct 6 (JxM, D1−D4)] suggesting a role for histidine residues in both IRAP metal binding sites (n = 3). (B) Aminopeptidase activity of the histidine mutants measured by following Leu-MCA degradation. (C and D) Proposed allosteric zinc binding site in D4 with putative ligands, from left to right, His830, His934, His938, and His979 highlighted in purple.

of purified D1+D2, whether expressed individually or in the presence of D4, was significantly reduced in comparison to that of the full-length construct. This suggests that the decrease in activity observed for the catalytic region alone is not due to an altered affinity for the substrate but rather to the catalytic rate. This could indicate a requirement for D4 for full activity (i.e., D4 acts as an activator and/or regulator) or that a proportion of the population is inactive. The ligand binding B_{max} for D1+D2 (Figure 2B and Table 1) is similar to that of the complete extracellular domain, demonstrating that the reduced enzyme activity of D1+D2 is not due to a proportion of this construct being unfolded. D1+D2 was also much more sensitive to temperature and pH than the entire extracellular region (data not shown).

The role of D4 in regulating the activity of IRAP was explored further by measuring the activity of D1+D2 in the presence of D4. A small increase in the activity of D1+D2 was observed in the presence of D4, although not to the level found for the entire extracellular region construct (Table 2). This may be because of the low stability of the D1+D2 and D4 heterodimer or the interaction of the domains as separate molecules being only a partial mimic of the intact protein. This suggests that D4 is required to increase the level of stabilization and activity of D1+D2 and is consistent with the hypothesis that a conformational change of D4 upon binding of substrate may be involved in regulating the activity of D1+D2.

A surprising observation was that the presence of DTT substantially enhanced the activity of the full-length extracellular constructs (Table 2), with V_{max} only slightly increased but a substantially lower K_m for the synthetic substrate MCA. This suggested that DTT was acting by increasing the affinity for the substrate rather than enhancing the rate of the reaction. Radioligand binding of Ang IV in the presence of DTT also showed a significant increase in the affinity of the entire extracellular region for Ang IV in the presence of DTT (Figure 2C). By contrast, this phenomenon could not be detected with the catalytic domain constructs, indicating that the enhanced affinity seen in the presence of DTT required D3 and D4 (Figure 2D and Table 2). An alternative reducing agent, 2-mercaptoethanol, was tested to clarify whether it is the reducing action of DTT that enhances the activity of the full-length constructs. 2-Mercaptoethanol was able to increase the affinity of the full-length extracellular constructs for MCA, though not to the same extent as DTT (data not shown). This weaker effect could be a result of DTT's additional metal chelation enhancing affinity or differences in their reducing properties; however, it does suggest that the presence of a reducing agent does improve the affinity of IRAP for MCA, potentially through the

disruption of an internal disulfide bond enhancing access of the substrate to the catalytic site. Analysis of the metal content of the full-length constructs in the presence and absence of DTT or 2-mercaptoethanol revealed the same Zn^{2+} ion content.

The entire extracellular region of IRAP and constructs containing just D1+D2 were inhibited to the same extent by small molecule generic inhibitors amastatin and bestatin, specific and selective small molecule inhibitors HFI419, HFI435, and HFI437,[16] and peptide inhibitors Ang IV and LVV-H7 (Figure 2E and Table 2). Several of the constructs were designed to lack the juxtamembrane region previously proposed as the allosteric Ang IV binding site responsible for inhibition (constructs 3 and 8).[21] Inhibition of these constructs, however, was observed to approximately the same order of magnitude as seen in constructs containing this region (Table 2). This suggests that any allosteric binding site for Ang IV outside of D1+D2 of IRAP is not important for inhibition. Kinetic modeling showed that Ang IV competitively inhibited the activity of both the full-length extracellular region and the catalytic region ($R^2 = 0.98$) (data not shown).

We found that Ang IV binds to only constructs containing D1+D2 as judged by binding of ^{125}I-labeled Nle^1-Ang IV to each of the constructs (Figure 2C,D and Table 1), consistent with our kinetic data showing that Ang IV is binding directly to the catalytic site. Specific binding of radioligand was observed only in the presence of chelator. The presence of DTT was, however, able to improve the binding efficiency (by approximately 200%) of the full-length constructs but not that of the catalytic constructs (Figure 2C). To rule out any effect of iodination on the binding properties of Ang IV, the ability of ^{125}I-labeled Nle^1-Ang IV to inhibit the catalytic activity of IRAP was examined. The iodinated Nle^1-Ang IV did not show any significant difference in its inhibition of unlabeled Nle^1-Ang IV. Analysis of the binding curves showed no indication of cooperativity between the two monomers, with the caveat that the measurements were taken in the absence of Zn^{2+}.

Identification of a Second Noncatalytic Zinc Site. ICP-MS was used to examine the Zn content in the purified protein and indicated that there were two Zn^{2+} ions per monomer in the full-length extracellular construct (Table 1). Upon addition of excess Ang IV to the full-length extracellular constructs, one Zn^{2+} was lost. The models of IRAP were then uploaded to the Stanford Feature Metal Scan analysis model[56] that correctly identified the catalytic zinc binding site in the models of both the open and closed forms and predicted another potential zinc binding site toward the C-terminus of the open model, with two potential sets of coordinating residues consisting of E825, C828, and C835 and H830, H934, and H938.

Examination of individual domain fragments by ICP-MS indicated that one Zn^{2+} was associated with D1+D2 and the other with D4, consistent with the Feature Metal Scan prediction. Loss of zinc was not observed when Ang IV was added to the catalytic domain constructs (Table 1), suggesting that it is the Zn^{2+} associated with D4 that was lost, consistent with the hypothesis that D4 undergoes a conformational change following binding of the peptide inhibitor. The effect of other IRAP ligands and substrates on zinc binding was also explored. While not as marked as that with Ang IV, loss of the second Zn^{2+} ion was observed with small molecule inhibitors HFI419, HFI435, and HFI437, and a reduction of approximately 75% of the second Zn^{2+} ion was observed for the full-length extracellular constructs upon addition of excess substrates MCA, oxytocin, and vasopressin; however, no loss of zinc from the catalytic domain constructs was seen (Table S2 of the Supporting Information).

To further explore this novel Zn^{2+} binding site, we examined the pH dependence of Zn^{2+} binding by the purified constructs. This revealed that the two sites had similar profiles, with all zinc lost at pH ~6.2, approximately the normal pK_a of histidine residues (Figure 3A). This correlated with the pH sensitivity of the activity of the constructs as all enzyme function was lost around pH 6.2. While the catalytic Zn^{2+} binding motif has been well characterized and is known to contain two histidines, these data suggest that histidine residues are also involved in the chelation of the second zinc. Therefore, to identify some of the residues that are important in this second Zn^{2+} binding site, we mutated all histidine residues to alanines and expressed and purified them from insect cells for biochemical analysis (Table S3 of the Supporting Information). Five of the purified histidine-mutated constructs exhibited significant changes in zinc content, H464A, H468A, H830A, H934A, and H938A. Histidines 464 and 468 are the "catalytic histidines" responsible for coordinating the zinc ion in the active site and have both been characterized previously.[57] Consistent with their role in the active site and the previous characterization of their mutation, H464A and H468A both lacked any measurable aminopeptidase activity (Table S3 of the Supporting Information). Mutations in the three other histidine residues decreased the amount of zinc bound but did not dramatically alter the aminopeptidase activity (Table S3 of the Supporting Information and Figure 3B). These histidines are clustered toward the distal end of D4 (Figure 3C,D). Inspection of both models of IRAP identified that this cluster of histidines could potentially bind a Zn^{2+} ion with coordinating ligands H830, H934, and H938 or H934, H938, and H979. We consider the former more plausible, because it is consistent with the predictions from the Stanford Feature Metal Scan and the H979A mutation resulted in an only partial reduction in the level of zinc binding, potentially through a localized allosteric effect.

DISCUSSION

In this study, we have used insect cells to express and purify a range of soluble recombinant IRAP fragments and mutants to gain a better understanding of the biochemical mechanisms underlining its regulation and inhibition, particularly with regard to behavior of the hexapeptide inhibitor Ang IV. While Ang IV has been shown to significantly improve memory, the exact mechanism of how it exerts this through binding to IRAP is still being debated in the literature. The rational development of therapeutic agents to mimic the effects of Ang IV requires a more detailed understanding of this mechanism. Apart from one study by Matsumoto and colleagues of the full-length extracellular enzyme,[58] all characterizations of IRAP have been conducted on partially purified preparations from mammalian cells requiring membrane micelles for solubilization.

In this study, we have demonstrated that IRAP exists as a noncovalent homodimer. Two members of the M1 aminopeptidase family, APA and TRH-DE, have been shown to exist as disulfide-linked homodimers with the cysteine residue adjacent to the transmembrane domain identified as the amino acid involved in the covalent bond.[53,59] While IRAP contains a corresponding cysteine residue, complete dimerization was observed even in constructs lacking this region, demonstrating that IRAP dimerizes through a different mechanism.

All constructs that contained the catalytic region (D1+D2) were sufficient for activity and could be inhibited by amastatin, bestatin, Ang IV, and LVV-H7. The activity of the catalytic regions, however, was dramatically lower than for the full-length extracellular constructs, suggesting that the C-terminal region is required for full activity. Indeed, we observed an increase in activity when isolated D4 was added to the D1+D2 construct, although not to the levels of the full-length intact extracellular constructs. Other groups have attempted to examine the role of the catalytic region of M1 aminopeptidases by expressing just the catalytic region in mammalian cells but failed to observe activity.[60,61] Recently, catalytic regions generated by proteolysis of intact aminopeptidases or by coexpression with the C-terminal region have exhibited some activity.[60,62] Thus, the C-terminal region appears to be essential for correct processing and folding in mammalian cells. Kumar and colleagues[63] showed that removal of just a few amino acid residues from the C-terminal region of the bacterial M1 aminopeptidases Tricorn Interacting Factor F2 and Peptidase N greatly reduced activity, which highlighted the importance of this domain for activity.

Here we have definitively shown that Ang IV binds to and competitively inhibits the catalytic domain and activity of IRAP, and there is no evidence that Ang IV binds to some allosteric site. We saw the same levels of both activity and inhibition by Ang IV in the presence and absence of the juxtamembrane region previously proposed as an allosteric binding site of Ang IV.[21] Furthermore, [^{125}I]Ang IV was shown to bind in an approximately 1:1 ratio to all of the constructs containing the catalytic region, suggesting that there is only one Ang IV binding site and it is not located in the juxtamembrane region or in the C-terminal region. This is consistent with the kinetic modeling that indicated Ang IV inhibition was competitive. We still did observe a significant difference in affinity between inhibition of catalytic activity and binding in the presence of divalent cation chelators. This does not necessarily indicate that Ang IV binds to only the apoenzyme but that we can measure binding to only the apoenzyme. This could be a reflection of different mechanisms of binding, that the removal of zinc is able to help further stabilize Ang IV binding and/or differences in binding affinity between the native (~100 nM) and apoenzyme (~10 nM) particularly as weaker affinity binding can easily be missed by radioligand binding experiments.

Interestingly, iodination of the phenolic ring of the Tyr residue in Nle^1-Ang IV[64] did not affect the potency of inhibition within the catalytic assays. This is in contrast to the results of several studies that have proposed that iodinated Ang IV may exhibit behavior different from that of noniodinated Ang IV[24] and the observation that the tyrosine residue plays an important role in the binding to IRAP.[65,66] These proposals have been based on radiolabeled binding and competition studies using iodinated Ang IV, in the presence of metal chelators, and comparisons with inhibition potency of noniodinated ligands in activity assays. However, the binding efficiencies in the radioligand binding assays of both iodinated and noniodinated Nle^1-Ang IV are fairly similar, which would indicate that under the same conditions they behave in a similar manner. This was further confirmed when we directly compared iodinated and noniodinated ligands in a kinetic assay and saw no significant difference in the ability to inhibit catalytic activity. Furthermore, on the basis of docking studies, if Ang IV binds to IRAP in the manner we believe likely, there is room in the pocket surrounding the tyrosine residue to accept the large, hydrophobic iodine atom. We believe this supports our hypothesis that the difference in affinity observed between the radioligand binding studies and kinetic assays is a result of the assay conditions selecting between a zinc-depleted apo form and a catalytically active form.

Limited proteolysis of the full-length extracellular constructs revealed the formation of two stable proteins, one corresponding to D1+D2 and the other to D4. However, neither of these fragments contained the interstitial β-sheet region (D3). In the presence of Ang IV, the full-length constructs were significantly more resilient to proteolysis, consistent with the proposal that the two regions undergo a conformational change upon binding substrate and/or inhibitor. Because labeled Ang IV bound only in the presence of metal chelators, we also tested the proteolytic sensitivity of the full-length constructs in the presence of 1,10-phenanthroline and saw no difference. However, the addition of Ang IV did not reduce the sensitivity of IRAP to proteolysis in the presence of a metal chelator. This suggests that Ang IV is binding in a different way in the presence of metal chelators and could explain the differences observed between the binding affinities and inhibition constants.

We observed that a reducing agent increased not only the affinity of the full-length extracellular region for [^{125}I]Ang IV but also the activity measured by hydrolysis of MCA, building upon a previous observation.[67] The redox state may play a role in the regulation of IRAP activity in vivo, with activity lost over time while in the oxidizing environment of the cell surface.

On the basis of recent crystal structures, it was proposed that conformational changes of the C-terminal region of APN might regulate activity,[45] whereby the extracellular region might adopt an "open" and "closed" conformation with the C-terminal region pivoting on a "hinge". As part of the mechanism of moving from an open conformation to a closed conformation, Ito and coworkers[45] proposed that a small movement of catalytic residues occurred, generating a catalytically competent active site. Our observation that DTT was able to enhance activity and Ang IV binding only in the presence of the C-terminal domain may be a result of an interaction between D4 and the active site. Our open inactive state model of IRAP predicts that C828 and C835 could form a disulfide bond whereas such a bond is not possible in our closed active state model, thus providing a molecular basis for understanding the effect of a reducing agent on IRAP activity (Figure S3 of the Supporting Information). Such a model is fully consistent with our observation that the full-length extracellular construct was significantly more resilient to proteolysis in the presence of Ang IV.

When we examined the Zn^{2+} content in our purified extracellular region constructs, we were surprised to find two Zn^{2+} ions bound per monomer, as it had been previously shown there was only one site[58] and there were no reports of a second zinc binding site in other M1 aminopeptidases. It is likely that the second site was missed because, unlike here, the protein was expressed and purified without the addition of Zn^{2+}.[58] In addition to the Zn^{2+} ion in the active site, we found that constructs containing the isolated C-terminal region contained the second Zn^{2+} site. In silico scanning of the models of IRAP revealed two potential coordination clusters in D4 of the open state model (but none in the closed active state model). Mutation of histidine residues indicated the likely binding site for the Zn^{2+} ion was toward the distal end of D4 with coordinating residues H830, H934, and H938. It remains to be established whether this second site is physiologically relevant. There have been reports of other bivalent metal ions regulating the activity of M1 aminopeptidases, including calcium in APA[68,69] and

magnesium and calcium in IRAP and APN,[22,54,70] although none of these metals would be expected to bind to histidine residues. Nevertheless, the second zinc site proved to be a useful reporter of possible conformational changes; for example, in the presence of Ang IV, this Zn^{2+} ion is lost, suggesting conformational changes have taken place, consistent with our observation that extracellular constructs were more protease resistant in the presence of Ang IV, whereas in the absence of the inhibitor, the constructs were readily degraded to separate N-terminal and C-terminal products.

In summary, our results support the hypothesis that IRAP is composed of distinct domains that undergo interdomain conformational changes that allow the extracellular region of IRAP to adopt an open inactive state or a closed active state. In the absence of the C-terminal domain, there is greatly reduced activity consistent with this domain playing a role in the regulation of IRAP activity.

■ ASSOCIATED CONTENT

Supporting Information. Mass spectrometry analysis of two stable fragments produced by the partial proteolysis of the extracellular region of IRAP (Table S1), zinc content in the presence of excess substrates and inhibitors (Table S2), role of IRAP histidine residues in zinc binding (Table S3), sequence alignments guiding molecular model building and domain prediction (Figure S1), SDS−PAGE gels showing the generation of stable fragments through partial proteolysis and pull-down assays to assay for interactions between expressed stable fragments (Figure S2), and positions of Cys828 and Cys835 (purple) in the open and closed molecular models (left and right panels, respectively) (Figure S3). This material is available free of charge via the Internet at http://pubs.acs.org.

■ AUTHOR INFORMATION

Corresponding Author

*Biota Structural Biology Laboratory, St. Vincent's Institute, 9 Princes St., Fitzroy, Victoria 3065, Australia. Telephone: 61-3-9288-2499. Fax: 61-3-9416-2676. E-mail: mparker@svi.edu.au.

Funding Sources

This work was supported by a grant from the National Health and Medical Research Council of Australia (NHMRC) to S.Y.C. and M.W.P. D.B.A. was an Australian Postgraduate Award Scholar and the recipient of a St. Vincent's Institute Foundation Scholarship sponsored by Colin North and Major Engineering. S.Y.C. was supported by an NHMRC Senior Research Fellowship. M.W.P. is an Australian Research Council Federation Fellow and an NHMRC Honorary Fellow.

■ ABBREVIATIONS

1,10-PHE, 1,10-phenanthroline; A-LAP, adipocyte-derived leucine aminopeptidase; Ang IV, angiotensin IV; APA, aminopeptidase A; APN, aminopeptidase N; DTT, dithiothreitol; EDTA, ethylenediaminetetraacetic acid; EGTA, ethylene glycol tetraacetic acid; GLUT4, glucose transporter 4; HBM, honey bee melettin; ICP-MS, inductively coupled plasma mass spectrometry; IMAC, immobilized metal affinity chromatography; IRAP, insulin-regulated membrane aminopeptidase; L-RAP, leukocyte-derived arginine aminopeptidase; LTA4H, leukotriene A4 hydrolase; LVV-H7, Leu-Val-Val-hemorphin-7; MCA, 4-methylcoumaryl-7-amide; MS, mass spectrometry; Nle, norleucine; SEC, size exclusion chromatography; TEV, tobacco etch virus; TOF-MS, time-of-flight mass spectrometry; TRH-DE, thyrotropin-releasing hormone degrading enzyme.

■ REFERENCES

(1) Albiston, A. L., McDowall, S. G., Matsacos, D., Sim, P., Clune, E., Mustafa, T., Lee, J., Mendelsohn, F. A., Simpson, R. J., Connolly, L. M., and Chai, S. Y. (2001) Evidence that the angiotensin IV (AT_4) receptor is the enzyme insulin-regulated aminopeptidase. *J. Biol. Chem. 276*, 48623–48626.

(2) Rogi, T., Tsujimoto, M., Nakazato, H., Mizutani, S., and Tomoda, Y. (1996) Human placental leucine aminopeptidase/oxytocinase. A new member of type II membrane-spanning zinc metallopeptidase family. *J. Biol. Chem. 271*, 56–61.

(3) Segura, E., Albiston, A. L., Wicks, I. P., Chai, S. Y., and Villadangos, J. A. (2009) Different cross-presentation pathways in steady-state and inflammatory dendritic cells. *Proc. Natl. Acad. Sci. U.S. A. 106*, 20377–20381.

(4) Saveanu, L., Carroll, O., Weimershaus, M., Guermonprez, P., Firat, E., Lindo, V., Greer, F., Davoust, J., Kratzer, R., Keller, S. R., Niedermann, G., and van Endert, P. (2009) IRAP identifies an endosomal compartment required for MHC class I cross-presentation. *Science 325*, 213–217.

(5) Albiston, A. L., Peck, G. R., Yeatman, H. R., Fernando, R., Ye, S., and Chai, S. Y. (2007) Therapeutic targeting of insulin-regulated aminopeptidase: Heads and tails?. *Pharmacol. Ther. 116*, 417–427.

(6) Lew, R. A., Mustafa, T., Ye, S., McDowall, S. G., Chai, S. Y., and Albiston, A. L. (2003) Angiotensin AT4 ligands are potent, competitive inhibitors of insulin regulated aminopeptidase (IRAP). *J. Neurochem. 86*, 344–350.

(7) Lee, J., Mustafa, T., McDowall, S. G., Mendelsohn, F. A., Brennan, M., Lew, R. A., Albiston, A. L., and Chai, S. Y. (2003) Structure-activity study of LVV-hemorphin-7: Angiotensin AT4 receptor ligand and inhibitor of insulin-regulated aminopeptidase. *J. Pharmacol. Exp. Ther. 305*, 205–211.

(8) Wright, J. W., Miller-Wing, A. V., Shaffer, M. J., Higginson, C., Wright, D. E., Hanesworth, J. M., and Harding, J. W. (1993) Angiotensin II(3−8) (ANG IV) hippocampal binding: Potential role in the facilitation of memory. *Brain Res. Bull. 32*, 497–502.

(9) Wright, J. W., Stubley, L., Pederson, E. S., Kramar, E. A., Hanesworth, J. M., and Harding, J. W. (1999) Contributions of the brain angiotensin IV-AT4 receptor subtype system to spatial learning. *J. Neurosci. 19*, 3952–3961.

(10) Wright, J. W., Clemens, J. A., Panetta, J. A., Smalstig, E. B., Weatherly, L. A., Kramar, E. A., Pederson, E. S., Mungall, B. H., and Harding, J. W. (1996) Effects of LY231617 and angiotensin IV on ischemia-induced deficits in circular water maze and passive avoidance performance in rats. *Brain Res. 717*, 1–11.

(11) Pederson, E. S., Harding, J. W., and Wright, J. W. (1998) Attenuation of scopolamine-induced spatial learning impairments by an angiotensin IV analog. *Regul. Pept. 74*, 97–103.

(12) Pederson, E. S., Krishnan, R., Harding, J. W., and Wright, J. W. (2001) A role for the angiotensin AT4 receptor subtype in overcoming scopolamine-induced spatial memory deficits. *Regul. Pept. 102*, 147–156.

(13) Olson, M. L., Olson, E. A., Qualls, J. H., Stratton, J. J., Harding, J. W., and Wright, J. W. (2004) Norleucine1-Angiotensin IV alleviates mecamylamine-induced spatial memory deficits. *Peptides 25*, 233–241.

(14) Gulpinar, M. A., and Yegen, B. C. (2004) The physiology of learning and memory: Role of peptides and stress. *Curr. Protein Pept. Sci. 5*, 457–473.

(15) Chai, S. Y., Fernando, R., Peck, G., Ye, S. Y., Mendelsohn, F. A., Jenkins, T. A., and Albiston, A. L. (2004) The angiotensin IV/AT4 receptor. *Cell. Mol. Life Sci. 61*, 2728–2737.

(16) Albiston, A. L., Morton, C. J., Ng, H. L., Pham, V., Yeatman, H. R., Ye, S., Fernando, R. N., De Bundel, D., Ascher, D. B., Mendelsohn, F. A., Parker, M. W., and Chai, S. Y. (2008) Identification and characterization of a new cognitive enhancer based on inhibition of insulin-regulated aminopeptidase. *FASEB J. 22*, 4209–4217.

(17) Iwase, A., Nomura, S., and Mizutani, S. (2001) Characterization of a secretase activity for placental leucine aminopeptidase. *Arch. Biochem. Biophys. 393*, 163–169.

(18) Ofner, L. D., and Hooper, N. M. (2002) Ectodomain shedding of cystinyl aminopeptidase from human placental membranes. *Placenta 23*, 65–70.

(19) Ito, N., Nomura, S., Iwase, A., Ito, T., Kikkawa, F., Tsujimoto, M., Ishiura, S., and Mizutani, S. (2004) ADAMs, a disintegrin and metalloproteinases, mediate shedding of oxytocinase. *Biochem. Biophys. Res. Commun. 314*, 1008–1013.

(20) Ye, S., Chai, S. Y., Lew, R. A., and Albiston, A. L. (2007) Insulin-regulated aminopeptidase: Analysis of peptide substrate and inhibitor binding to the catalytic domain. *Biol. Chem. 388*, 399–403.

(21) Caron, A. Z., Arguin, G., and Guillemette, G. (2003) Angiotensin IV interacts with a juxtamembrane site on AT_4/IRAP suggesting an allosteric mechanism of enzyme modulation. *Regul. Pept. 113*, 9–15.

(22) Demaegdt, H., Laeremans, H., De Backer, J. P., Mosselmans, S., Le, M. T., Kersemans, V., Michotte, Y., Vauquelin, G., and Vanderheyden, P. M. (2004) Synergistic modulation of cystinyl aminopeptidase by divalent cation chelators. *Biochem. Pharmacol. 68*, 893–900.

(23) Demaegdt, H., Lenaerts, P. J., Swales, J., De Backer, J. P., Laeremans, H., Le, M. T., Kersemans, K., Vogel, L. K., Michotte, Y., Vanderheyden, P., and Vauquelin, G. (2006) Angiotensin AT4 receptor ligand interaction with cystinyl aminopeptidase and aminopeptidase N: [^{125}I]Angiotensin IV only binds to the cystinyl aminopeptidase apoenzyme. *Eur. J. Pharmacol. 546*, 19–27.

(24) Demaegdt, H., Lukaszuk, A., De Buyser, E., De Backer, J. P., Szemenyei, E., Toth, G., Chakravarthy, S., Panicker, M., Michotte, Y., Tourwe, D., and Vauquelin, G. (2009) Selective labeling of IRAP by the tritiated AT_4 receptor ligand [^{3}H]Angiotensin IV and its stable analog [^{3}H]AL-11. *Mol. Cell. Endocrinol. 311*, 77–86.

(25) Altschul, S. F., and Koonin, E. V. (1998) Iterated profile searches with PSI-BLAST: A tool for discovery in protein databases. *Trends Biochem. Sci. 23*, 444–447.

(26) Chenna, R., Sugawara, H., Koike, T., Lopez, R., Gibson, T. J., Higgins, D. G., and Thompson, J. D. (2003) Multiple sequence alignment with the Clustal series of programs. *Nucleic Acids Res. 31*, 3497–3500.

(27) Shi, J., Blundell, T. L., and Mizuguchi, K. (2001) FUGUE: Sequence-structure homology recognition using environment-specific substitution tables and structure-dependent gap penalties. *J. Mol. Biol. 310*, 243–257.

(28) Barton, G. J. (1993) ALSCRIPT: A tool to format multiple sequence alignments. *Protein Eng. 6*, 37–40.

(29) Gouet, P., Courcelle, E., Stuart, D. I., and Metoz, F. (1999) ESPript: Analysis of multiple sequence alignments in PostScript. *Bioinformatics 15*, 305–308.

(30) Raghava, G. P. S. (2002) APSSP2: A combination method for protein secondary structure prediction based on neural network and example based learning. *CASP5*, A-132.

(31) Meiler, J., Müller, M., Zeidler, A., and Schmaeschke, F. (2001) Generation and Evaluation of Dimension Reduced Amino Acid Parameter Representations by Artificial Neural Networks. *J. Mol. Model. 7*, 360–369.

(32) Rost, B. (1996) PHD: Predicting one-dimensional protein structure by profile based neural networks. *Methods Enzymol. 266*, 525–539.

(33) Pasquier, C., and Hamodrakas, S. J. (1999) An hierarchical artificial neural network system for the classification of transmembrane proteins. *Protein Eng. 12*, 631–634.

(34) Jones, D. T. (1999) Protein secondary structure prediction based on position-specific scoring matrices. *J. Mol. Biol. 292*, 195–202.

(35) Cheng, J., Randall, A. Z., Sweredoski, M., and Baldi, P. (2005) SCRATCH: A Protein Structure and Structural Feature Prediction Server. *Nucleic Acids Res. 33*, 72–76.

(36) Tusnady, G. E., and Simon, I. (2001) The HMMTOP transmembrane topology prediction server. *Bioinformatics 17*, 849–850.

(37) Hirokawa, T., Boon-Chieng, S., and Mitaku, S. (1998) SOSUI: Classification and secondary structure prediction system for membrane proteins. *Bioinformatics 14*, 378–379.

(38) Milpetz, F., Argos, P., and Persson, B. (1995) TMAP: A new email and WWW service for membrane-protein structural predictions. *Trends Biochem. Sci. 20*, 204–205.

(39) Krogh, A., Larsson, B., von Heijne, G., and Sonnhammer, E. L. (2001) Predicting transmembrane protein topology with a hidden Markov model: Application to complete genomes. *J. Mol. Biol. 305*, 567–580.

(40) Hofmann, K., and Stoffel, W. (1993) TMbase: A database of membrane spanning proteins segments. *Biol. Chem. Hoppe-Seyler*, 374.

(41) Kanaoka, Y., Takahashi, T., and Nakayama, H. (1977) A new fluorogenic substrate for aminopeptidase. *Chem. Pharm. Bull. 25*, 362–363.

(42) Moeller, I., Lew, R. A., Mendelsohn, F. A., Smith, A. I., Brennan, M. E., Tetaz, T. J., and Chai, S. Y. (1997) The globin fragment LVV-hemorphin-7 is an endogenous ligand for the AT4 receptor in the brain. *J. Neurochem. 68*, 2530–2537.

(43) Wilkins, M. R., Lindskog, I., Gasteiger, E., Bairoch, A., Sanchez, J. C., Hochstrasser, D. F., and Appel, R. D. (1997) Detailed peptide characterization using PEPTIDEMASS: A World-Wide-Web-accessible tool. *Electrophoresis 18*, 403–408.

(44) Kyrieleis, O. J., Goettig, P., Kiefersauer, R., Huber, R., and Brandstetter, H. (2005) Crystal structures of the tricorn interacting factor F3 from *Thermoplasma acidophilum*, a zinc aminopeptidase in three different conformations. *J. Mol. Biol. 349*, 787–800.

(45) Ito, K., Nakajima, Y., Onohara, Y., Takeo, M., Nakashima, K., Matsubara, F., Ito, T., and Yoshimoto, T. (2006) Crystal structure of aminopeptidase N (proteobacteria alanyl aminopeptidase) from *Escherichia coli* and conformational change of methionine 260 involved in substrate recognition. *J. Biol. Chem. 281*, 33664–33676.

(46) Guex, N., and Peitsch, M. C. (1997) SWISS-MODEL and the Swiss-PdbViewer: An environment for comparative protein modeling. *Electrophoresis 18*, 2714–2723.

(47) Bowie, J. U., Luthy, R., and Eisenberg, D. (1991) A method to identify protein sequences that fold into a known three-dimensional structure. *Science 253*, 164–170.

(48) Thunnissen, M. M., Andersson, B., Samuelsson, B., Wong, C. H., and Haeggstrom, J. Z. (2002) Crystal structures of leukotriene A4 hydrolase in complex with captopril and two competitive tight-binding inhibitors. *FASEB J. 16*, 1648–1650.

(49) Nocek, B., Mulligan, R., Bargassa, M., Collart, F., and Joachimiak, A. (2008) Crystal structure of aminopeptidase N from human pathogen *Neisseria meningitidis*. *Proteins 70*, 273–279.

(50) Ye, S., Chai, S. Y., Lew, R. A., Ascher, D. B., Morton, C. J., Parker, M. W., and Albiston, A. L. (2008) Identification of modulating residues defining the catalytic cleft of insulin-regulated aminopeptidase. *Biochem. Cell Biol. 86*, 251–261.

(51) Hussain, M. M., Tranum-Jensen, J., Noren, O., Sjostrom, H., and Christiansen, K. (1981) Reconstitution of purified amphiphilic pig intestinal microvillus aminopeptidase. Mode of membrane insertion and morphology. *Biochem. J. 199*, 179–186.

(52) Danielsen, E. M. (1990) Biosynthesis of intestinal microvillar proteins. Dimerization of aminopeptidase N and lactase-phlorizin hydrolase. *Biochemistry 29*, 305–308.

(53) Papadopoulos, T., Heuer, H., and Bauer, K. (2000) Analysis of the thyrotropin-releasing hormone-degrading ectoenzyme by site-directed mutagenesis of cysteine residues. Cys68 is involved in disulfide-linked dimerization. *Eur. J. Biochem. 267*, 2617–2623.

(54) Laeremans, H., Demaegdt, H., De Backer, J. P., Le, M. T., Kersemans, V., Michotte, Y., Vauquelin, G., and Vanderheyden, P. M. (2005) Metal ion modulation of cystinyl aminopeptidase. *Biochem. J. 390*, 351–357.

(55) Demaegdt, H., Smitz, L., De Backer, J. P., Le, M. T., Bauwens, M., Szemenyei, E., Toth, G., Michotte, Y., Vanderheyden, P., and Vauquelin, G. (2008) Translocation of the insulin-regulated aminopeptidase to the cell surface: Detection by radioligand binding. *Br. J. Pharmacol. 154*, 872–881.

(56) Ebert, J. C., and Altman, R. B. (2008) Robust recognition of zinc binding sites in proteins. *Protein Sci. 17*, 54–65.

(57) Laustsen, P. G., Vang, S., and Kristensen, T. (2001) Mutational analysis of the active site of human insulin-regulated aminopeptidase. *Eur. J. Biochem. 268*, 98–104.

(58) Matsumoto, H., Rogi, T., Yamashiro, K., Kodama, S., Tsuruoka, N., Hattori, A., Takio, K., Mizutani, S., and Tsujimoto, M. (2000) Characterization of a recombinant soluble form of human placental leucine aminopeptidase/oxytocinase expressed in Chinese hamster ovary cells. *Eur. J. Biochem. 267*, 46–52.

(59) Hesp, J. R., and Hooper, N. M. (1997) Proteolytic fragmentation reveals the oligomeric and domain structure of porcine aminopeptidase A. *Biochemistry 36*, 3000–3007.

(60) Rozenfeld, R., Muller, L., El Messari, S., and Llorens-Cortes, C. (2004) The C-terminal domain of aminopeptidase A is an intramolecular chaperone required for the correct folding, cell surface expression, and activity of this monozinc aminopeptidase. *J. Biol. Chem. 279*, 43285–43295.

(61) Ofner, L. D., and Hooper, N. M. (2002) The C-terminal domain, but not the interchain disulphide, is required for the activity and intracellular trafficking of aminopeptidase A. *Biochem. J. 362*, 191–197.

(62) Ma, Z., Daquin, A., Yao, J., Rodgers, D., Thompson, M. W., and Hersh, L. B. (2003) Proteolytic cleavage of the puromycin-sensitive aminopeptidase generates a substrate binding domain. *Arch. Biochem. Biophys. 415*, 80–86.

(63) Kumar, A., Bhosale, M., Reddy, S., Srinivasan, N., and Nandi, D. (2009) Importance of non-conserved distal carboxyl terminal amino acids in two peptidases belonging to the M1 family: *Thermoplasma acidophilum* Tricorn interacting factor F2 and *Escherichia coli* Peptidase N. *Biochimie 91*, 1145–1155.

(64) Lahoutte, T., Mertens, J., Caveliers, V., Franken, P. R., Everaert, H., and Bossuyt, A. (2003) Comparative biodistribution of iodinated amino acids in rats: Selection of the optimal analog for oncologic imaging outside the brain. *J. Nucl. Med. 44*, 1489–1494.

(65) Sardinia, M. F., Hanesworth, J. M., Krebs, L. T., and Harding, J. W. (1993) AT4 receptor binding characteristics: D-Amino acid- and glycine-substituted peptides. *Peptides 14*, 949–954.

(66) Sardinia, M. F., Hanesworth, J. M., Krishnan, F., and Harding, J. W. (1994) AT4 receptor structure-binding relationship: N-terminal-modified angiotensin IV analogues. *Peptides 15*, 1399–1406.

(67) Jarvis, M. F., and Gessner, G. W. (1994) Dithiothreitol, sodium chloride, and ethylenediaminetetraacetic acid increase the binding affinity of [^{125}I]angiotensin IV to AT4 receptors in bovine adrenal cortex. *Peptides 15*, 1037–1044.

(68) Iturrioz, X., Vazeux, G., Celerier, J., Corvol, P., and Llorens-Cortes, C. (2000) Histidine 450 plays a critical role in catalysis and, with Ca^{2+}, contributes to the substrate specificity of aminopeptidase A. *Biochemistry 39*, 3061–3068.

(69) Goto, Y., Hattori, A., Mizutani, S., and Tsujimoto, M. (2007) Asparatic acid 221 is critical in the calcium-induced modulation of the enzymatic activity of human aminopeptidase A. *J. Biol. Chem. 282*, 37074–37081.

(70) Vanderheyden, P. M., Demaegdt, H., Swales, J., Lenaerts, P. J., De Backer, J. P., Vogel, L. K., and Vauquelin, G. (2006) Synergistic inhibition of the enzymatic activity of aminopeptidase N by divalent metal ion chelators. *Fundam. Clin. Pharmacol. 20*, 613–619.